Experimental evidence that polystyrene nanoplastics cross the intestinal barrier of European seabass

Marie Vagner, Gaëlle G. Boudry, Lucie Courcot, Dorothée Vincent, Alexandre Dehaut, Guillaume Duflos, Arnaud Huvet, Kévin Tallec, Jose-Luis Zambonino-Infante

Experimental evidence that polystyrene nanoplastics cross the intestinal barrier of European seabass

Vagner M.[1*], Boudry G.[2], Courcot L.[3], Vincent D.[4], Dehaut A.[5], Duflos G.[5], Huvet A.[1], Tallec K.[1], Zambonino-Infante J-L.[1]

[1]Univ Brest, CNRS, IRD, Ifremer, LEMAR, F-29280 Plouzané, France

[2]Institut Numecan, INRAE, INSERM, Univ Rennes, F-35590 Saint-Gilles, France

[3]Laboratoire d'Océanologie et de Géosciences, Université Littoral Côte d'Opale, University of Lille, CNRS, UMR 8187, LOG, 32 avenue Foch, F-62930 Wimereux, France

[4]Office Français de la Biodiversité (OFB), Direction Surveillance Évaluation et Données (DSUED), Service Écosystèmes Connaissances et Usages des milieux marins (ECUMM), 16 quai de la Douane, F-29200 Brest, France

[5]ANSES Laboratoire de Sécurité des Aliments, 6 Boulevard du Bassin Napoléon, F-62200 Boulogne-sur-Mer, France

* marie.vagner@univ-brest.fr

Highlights

- Plastic particles crossing the intestinal barrier is debated
- PS-NP particles were tested in ex-vivo time series experiments using Ussing chambers
- Two PS-NP concentrations were tested on two locations of adult Seabass guts
- PS-NP directly crossed the intestinal barrier of adult Seabass within few minutes
- PS-NP translocation was confirmed by 3 complementary techniques

Abstract

Plastic pollution in marine ecosystems constitutes an important threat to marine life. For vertebrates, macro/microplastics can obstruct and/or transit into the airways and digestive tract whereas nanoplastics (NPs; < 1000 nm) have been observed in non-digestive tissues such as the liver and brain. Whether NPs cross the intestinal epithelium to gain access to the blood and internal organs remains controversial, however. Here, we show directly NP translocation across the intestinal barrier of a fish, the European seabass, *Dicentrarchus labrax, ex vivo*. The luminal side of median and distal segments of intestine were exposed to fluorescent polystyrene NPs (PS-NPs) of 50 nm diameter. PS-NPs that translocated to the serosal side were then detected quantitatively by fluorimetry, and qualitatively by scanning electron microscopy (SEM) and pyrolysis coupled to gas chromatography and high-resolution mass spectrometry (Py-GC-HRMS). Fluorescence intensity on the serosal side increased 15–90 min after PS-NP addition into the luminal side, suggesting that PS-NPs crossed the intestinal barrier; this was confirmed by both SEM and Py-GC-HRMS. This study thus evidenced conclusively that NPs beads translocate across the intestinal epithelium in this marine vertebrate.

Key words: polystyrene nanoplastic beads, translocation, intestinal epithelium, *Dicentrarchus labrax*, Ussing chambers

1. Introduction

Whether plastic particles delivered through the food chain enter the circulation and reach organs by crossing the intestinal barrier, i.e. by translocation, remains a question of discussion (Catarino et al., 2019; Paul-Pont et al., 2018; Schür et al., 2019; Triebskorn et al., 2019). Almost 50 years ago, Volkheimer used histology and staining methods to show that during normal digestion in mammals, particles of about 1 µm passed between adjacent epithelial cells of the

intestine and entered the subepithelial compartment, from where they entered the bloodstream (Volkheimer, 1974). That study also found that particles up to 50 µm in diameter passed through enterocytes by a pinocytosis-like process. Later, Volkheimer showed that 5–110 µm particles of polyvinyl chloride appeared in the blood 2 h after ingestion by dogs, and smaller particles were translocated more rapidly than larger ones (Volkheimer, 1975). In fish, the translocation of plastic particles across the intestine has been implied by the discovery of particles in various tissues of several species (Collard et al., 2017; Elizalde-Velázquez et al., 2020; Jovanović et al., 2018; Kim et al., 2020; Mattsson et al., 2017; Zeytin et al., 2020), although the evidence is not indisputable. For example, the presence of two microplastic (MP) particles of 39 and 90 µm was reported in the livers of wild anchovy, *Engraulis encrasicolus* (Collard et al., 2017), but the precise location of the particles in or near blood cells could not be accurately inferred due to inadequate tissue preparation. Experimental studies have also suggested transfer of 200–600 µm MPs from the digestive tract to the liver in grey mullet, *Mugil cephalus*, and the presence of polystyrene (PS) particles (ranging from 214 to 288 µm) was observed in the livers of a few individual seabream, *Sparus aurata*, 45 days after their addition to the diet (Jovanović et al., 2018). In Crucian carp, *Carassius carassius*, fed food containing 53 nm and 180 nm polystyrene nanoplastic (PS-NPs) particles, the particles were detected in the brain by hyperspectral imaging (Mattsson et al., 2017). Similarly, in fathead minnow, *Pimephales promelas*, 60–70 nm PS-NPs were found in liver and kidney 48 h after their addition to the diet (Elizalde-Velázquez et al., 2020).

All these studies suggest that translocation explains the presence of plastic particles in the various digestive and non-digestive organs. Before reaching internal organs, plastic particles need to cross the intestinal barrier, i.e. the tight junction sealed-epithelial cell monolayer that faces the luminal side as well as the lamina propria housing numerous immune cells. Besides translocation across the intestine, other mechanisms, such the way some seaweeds accumulate

plastics by adherence (Gutow et al., 2016), have been suggested by some authors (Abbasi et al., 2018). Recent studies tried to demonstrate the passage of NPs from the digestive tract to organs by using fluorescently labelled plastic particles (Ding et al., 2018; Pitt et al., 2018a, 2018b; van Pomeren et al., 2017). Those studies are now considered inconclusive, however, because the authors did not control for possible leaching of the fluorescent dye from the NPs (Catarino et al., 2019; Schür et al., 2019). Indeed, commercial fluorescently labelled NPs do leach their fluorophores, and the fluorophore alone can accumulate within internal tissues, as seen in studies of zebrafish larvae (Catarino et al., 2019; Schür et al., 2019). Thus, in uptake and translocation studies simple measurements of fluorescence in the target tissue may be misleading. Very recently, accumulation of palladium-doped polystyrene was evidenced in the mucosa and muscularis layers of the whole intestine of salmon and potential passage in the blood was only found in the anterior intestine (Clark et al., 2022). These results based on an *ex-vivo* gut sac exposure system are a tremendous step forward but, at the same time, raise some questions about a passage only through the pyloric caeca of the anterior intestine, which would necessarily limit the scope of this observation only to species that have them (Barrington, 1957; Kapoor et al., 1976). Complementary and innovative methods are still needed to ascertain whether NPs cross the intestinal barrier (Paul-Pont et al., 2018).

Here, the passage of PS-NPs across the intestine of the European seabass, *Dicentrarchus labrax*, a temperate carnivorous fish of ecological and economic interest has been evaluated. We use an *ex vivo* approach, based on Ussing chambers (Ussing and Zerahn, 1951) recognized since a long time as an optimal method for studying transport/absorption processes in intestine of several species including fish (Ašmonaitė et al., 2018; Clarke, 2009; de Jonge et al., 2004; Grosell and Genz, 2006; Guffey et al., 2011; Haslam et al., 2011; Thomson et al., 2019; Weinrauch et al., 2021). Median and distal sections of intestine (mid- and hindgut) were exposed to two concentrations of 50 nm fluorescent PS-NPs on their luminal sides. To identify

particles that crossed the intestinal barrier, the serosal side was analyzed by using three complementary techniques: fluorescence measurement, visual inspection by scanning electron microscopy (SEM), and chemical analysis by high-resolution mass spectrometry (Py-GC-HRMS). Thus, we show directly the translocation of PS-NPs across the intestinal epithelium.

2. Materials and methods

Ethic statement: All fish manipulations were performed according to the Animal Care Committee of France (ACCF), and the authors complied with the ARRIVE guidelines.

2.1. *Polystyrene nanoplastics (PS-NP)*

Commercially available polystyrene nanoplastics (PS-NP) 50-nm beads at 5000 mg L^{-1} with a blue (excitation 358 nm and emission 410 nm) fluorescent label L0780-1 mL were purchased from Sigma-Aldrich (Saint Louis, USA), and stored at 4°C prior to experiments. Previous Raman microspectroscopy analysis confirmed the PS nature of the polymer (Tallec et al., 2018). PS-NP commercial suspensions were in ultrapure water (UW) with Tween-20© surfactant (<0.1%) to limit aggregation; Tween-20© had previously been demonstrated to be innocuous for marine invertebrates at this dose (Ostroumov, 2003). Based on previous Dynamic Light Scattering analyses (DLS), we decided to use beads with amine group functionalization (NH_2) because they remain at the nanometric scale: the 50-NH_2 suspension exhibited a nanometer-scale size (mean ± SD; 125.6 ± 0.2 nm) and a positive surface charge (mean ± SD; 13.2 ± 1.0 mV) in natural filtered seawater. Before each use, particles were vortexed to prevent particle aggregation and ensure good suspension homogenization. The *Z*-average (size; nm) and the ζ-potential (mean surface charge; mV) were determined by DLS (nano-Zetasizer ZS Malvern Instruments) (Tallec et al., 2019) in the four media used in this study (see the next material and

methods sections): (i) Ultrapure water, (ii) 10 mM Krebs-Glucose, (iii) 10 mM Krebs-Mannitol, (iv) trichloroacetic acid (TCA). The PS-NP suspensions were added in disposable folded capillary cells (DTS 1060C, Malvern Instruments; Final volume = 1 mL). All analyses were conducted in triplicates (13 runs and 10 sec measure^{-1} for *Z*-average; 40 runs and 10 sec measure^{-1} ζ-potential; concentration: 100 g m^{-3}). DLS measurements were performed as described by Tallec et al., 2019 with a nano-Zetasizer ZS (Malvern Instruments, UK) using an angle of 173° Backscatter, a temperature of 20 °C and an equilibration of 120 s. We used the implemented data analysis software to measure the mean size of particles/aggregates (Z-average; nm), the aggregation state and the mean surface charge (ζ-potential; mV) of NP. The accuracy of all measures was verified with the report quality from the implemented software and a counting rate being always higher than 100 kcps.

2.2. *Biological material and rearing conditions*

Fish used in this study were 23 healthy adult *Dicentrarchus labrax* individuals (about 1.5 kg, 2 males and 21 females) reared in an open circulating system at Ifremer (French Institute for Sea Exploration) facilities in Plouzané, France. Running seawater passed successively through a tungsten heater and a degassing column packed with plastic rings and the water parameters followed that of the environment during the experimental period (from October 2018 to November 2019). Water temperature (15°C ± 3°C), oxygen (99% ± 1%) and pH (8 ± 0.1) were controlled once a week using multiparameter WTW probes (OXI 340, and pH3310, respectively). Fish were fed *ad libitum* industrial food (Le Gouessant®, Lamballe, France) twice a week.

Portions of the median and distal intestine tested in the present study can be collected from the same animal.

2.3. *Ussing experiment*

2.3.1. *Experimental set-up*

The experimental set-up for Ussing experiment is presented in Fig. 1. It is composed of two glass half chambers: one luminal and one serosal between which the intestine is mounted as a flat sheet. Each half chamber is connected by a tubing system to a U-shaped reservoir filled with Krebs that was supplemented with 10 mM glucose on the serosal side to ensure energy provision to the intestinal cells and 10mM mannitol on the luminal side to counterbalance osmolarity. Ussing chambers compartments were carefully washed with filtered distilled water to avoid any potential plastic contamination. The 10 mM Krebs-Glucose was made with 1/11 vol. of 10X Krebs (NaCl: 1.16 M, KCl: 0.05 M, KH2PO4: 0.01 M, MgSO4-7H2O: 0.023 M, NaHCO3: 0.25 M) at pH 7.2, 1/100 vol. 10X CaCl2 at 0.0075 M, and 10 mM D-glucose. The 10 mM Krebs-Mannitol solution was made similarly, replacing the D-glucose by D-Mannitol. All chemicals were supplied by Sigma-Aldrich (Saint-Quentin Fallavier, France).

The area of exposure of the intestinal epithelium was 2.35 cm^2. Oxygenation and stirring of solutions were ensured by an air-lift on both sides of the intestinal segments.

Fig. 1

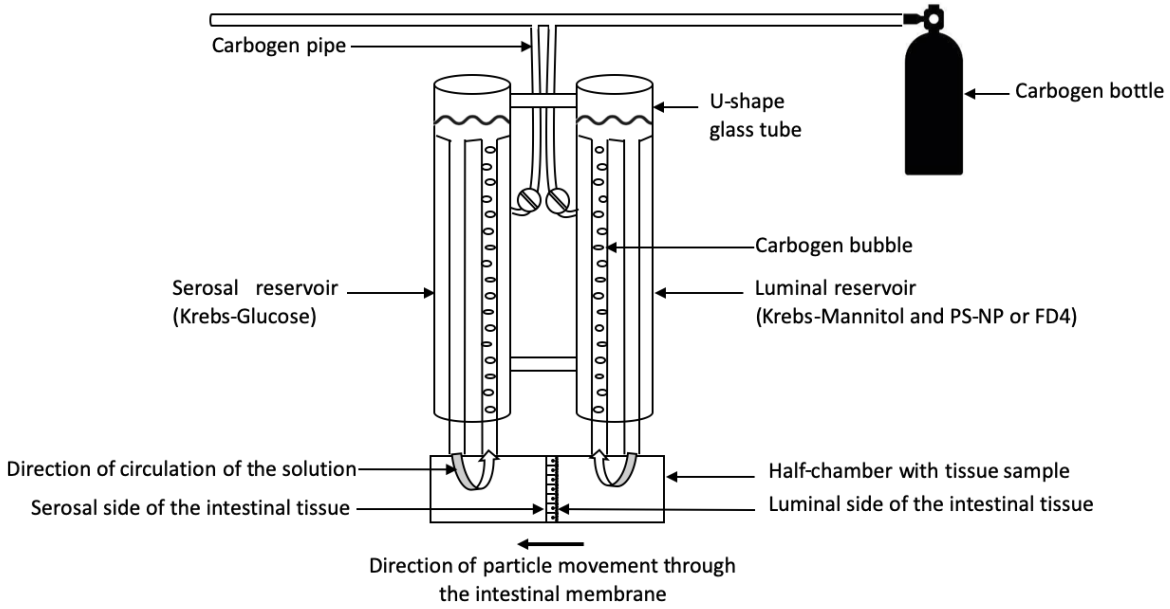

Fig. 1: Experimental set-up of a circulating Ussing device. It is composed of glass compartments. It contains two half chambers: one luminal and one serosal between which the intestine is mounted as a flat sheet. Two U-shaped reservoirs, filled with 8 mL oxygenated Krebs-Glucose (on the serosal side) or 8 mL Krebs-Mannitol (on the luminal side) are connected to each half chamber by a tubing system. Carbogen bottle contains 95% O_2 and 5% CO_2. The CO_2 aimed to buffer the Krebs solution that contains HCO_3^- and then helped to maintain a pH of 7.3 in each chamber. Polystyrene nanoplastic beads (PS-NP) or fluorescein isothiocyanate dextran 4000 molecule (FD4) were added to Krebs-Mannitol in the luminal part. The direction of circulation of the solutions is indicated for the two half-chambers. An arrow indicates the direction of potential particle movement from the luminal side to the serosal side of the intestinal membrane.

193 2.3.2. *Kinetic protocol*

194 Each day of experiment, one or two 72h-starved fish were euthanized by an anesthetic overdose
195 (Eugenol 1 mL L^{-1}; Fili@vet Reseau Cristal, France), and their intestine was entirely removed.
196 Then, the median or the distal segment were isolated.

197 Each portion of the intestine was then opened in order to obtain the luminal side on one face
198 and the serosal face on the other. The intestinal segments were mounted in Ussing chambers
199 (Fig.1), and 8 mL of Krebs-Mannitol and 8 mL of Krebs-Glucose solutions were added to the
200 luminal and serosal sides of the epithelium, respectively. The whole experiment was performed
201 at room temperature (approx. 20°C).

202 In order to study the transfer rate of an experimental substance across the epithelium, one
203 volume of Krebs-Mannitol was replaced by one volume of the experimental substance. Two
204 experimental substances were tested: i) the fluorescein isothiocyanate dextran 4000 molecule
205 (Sigma-Aldrich), which is an inert marker of gut permeability and integrity (Thomson et al.,
206 2019; molecular weight 3,000–5,000), hereafter called FD4, and ii) the PS-NP dispersions. A
207 volume of 200 µL of serosal Krebs-Glucose solution was sampled at T0 (just before adding the
208 experimental substance), and then at 15, 30, 45, 60, 90, 120, and 150 min after addition of the
209 experimental substance.

210

211 2.3.3. *Test for the integrity of the intestinal epithelium using FD4*

212 Because NPs themselves or the Tween added to the NP particles in order to prevent aggregation
213 could affect epithelial cells integrity, the integrity and the impermeability of the intestinal
214 epithelium to soluble macromolecules was determined by incubating the luminal side of median
215 or distal sections of fish intestine in the Ussing chamber (Fig. 1) with FD4, and with FD4
216 combined with two concentrations of 50-nm PS-NP fluorescent beads (20 mg L^{-1}, i.e. NP[20]
217 and 200 mg L^{-1}, i.e. NP[200], that are further used in the experiment; see 2.3.4). This test was

performed on 14 median (including 13 females and 1 male) and 15 distal intestinal segments (14 females and 1 male). One volume of Krebs-Mannitol was replaced by either the same volume of a FD4 solution (FD4 molecule diluted at 10 mg mL^{-1} in Krebs) in the luminal side (initial FD4 concentration in the luminal side: 125 µg mL^{-1}), or by one volume of FD4 + PS-NP. Then kinetic responses were measured, through the appearance of fluorescence on the serosal side at intervals up to 150 min (Fig. 2, and S5 for statistical results), and compared to T0.

A potential adsorption of FD4 was analyzed on the NPs to test if that might have modified the fluorescence of FD4, and thus have led to underestimate the presence of FD4 in the serosal side. The fluorescence of a calibration curve of FD4 (0, 62.5, 125, 500 ng mL^{-1}) was assayed in the absence or presence of PS-NPs added at each FD4 concentration tested at 20 mg L^{-1}, *i.e.* the largest PS-NP concentration we measured on the serosal side in our assays. FD4 fluorescence was read at 485/528 nm (excitation/emission), as described in the following 2.4.1. section. The regressions obtained from the calibration curves are not significantly different between FD4 alone or with NP addition (ANCOVA, p-value = 0.1814; see Supplementary Material S1). This result indicates that if there is any FD4 adsorption on NP, it does not result in any change in FD4 fluorescence.

2.3.4. *Test for the PS-NP transfer across the intestine using PS-NP beads*

To test for the passage of PS-NP across the intestinal epithelium, the luminal part of both median and distal segments of sea bass intestine was exposed to the two concentrations of 50 nm PS-NP fluorescent particles tested above (NP[20] and NP[200]). PS-NP transfer through the intestinal epithelium was tested by replacing one volume of Krebs-Mannitol in the luminal side by the same volume of the PS-NP dispersion stock (5000 mg L^{-1} diluted in 4 mL Krebs-Glucose). The PS-NP concentrations tested were based on the range of values reviewed for

exposure experiments of cationic amino polystyrene (PS-NH_2) on different phylum (from micro-algae to molluscs (Gonçalves and Bebianno, 2021):

- 20 mg L^{-1}, obtained by replacing 32 µL of Krebs-Mannitol by the same volume of PS-NP dispersion (5000 mg L^{-1} diluted in 4 mL Krebs-Glucose) to the luminal side (NP[20]: n=6 median and n=6 distal, including 6 females). This corresponds to 2.88x10e^8 particles mL^{-1} (Tallec et al., 2021).
- 200 mg L^{-1}, obtained by replacing 320 µL of Krebs-Mannitol by the same volume of PS-NP dispersion (5000 mg L^{-1} diluted in 4 mL Krebs-Glucose) to the luminal side (NP[200]: n=6 distal and n=6 median, including 2 females and 4 males). This corresponds to 2.88x10e^9 particles mL^{-1} (Tallec et al., 2021).

The choice of a model nanoparticle with spherical shape and surface functionalization available commercially was only driven by the fact that it stays at the nanometric scale, a necessity for testing translocation. The use of these non-environmental concentrations can be viewed as proof of concept producing ground-breaking data for testing translocation. At this stage, it does not suggest an environmental risk. The concentration used in our study were high compared to the highest concentration of microplastics reported at sea (e.g. 8 particles mL^{-1}; (Brandon et al., 2020) even if the nanoplastic concentrations in the ocean are expected to be higher than microplastics (Wagner and Reemtsma, 2019).

The leakage of dye was controlled using the dialysis technique described in Catarino et al. (2019). Briefly, 20 µl (at 5000 mg L^{-1}) of PS-NP was added in 5 Pur-A-Lyzer dialysis tubes (200 µL of Krebs-Mannitol) provided by the Pur-A-Lyzer™ Mini Dialysis Kit (Sigma-Aldrich, USA). After 1:30 of incubation, fluorescence was read in the total volume of the 5 replicates dialysis tubes at the PS-NP wavelength 360/460 nm (excitation/emission) as described in the following 2.4.1.

2.4. *Sample analyses*

2.4.1. *Fluorescence data*

The transport kinetics was then measured based on fluorescence in the serosal part of the intestine during 150 min, and the corresponding PS-NP concentration was calculated using calibration curves. For that, 100 µL of samples collected at each sampling time during the kinetics were immediately read in duplicates on a high-binding flat bottom 96-well black plates (Greiner bio-one, Les Ulis, France) with a fluorimeter (multi-detection microplate reader Synergy HT, BioTek, Colmar, France) equipped with the Gen5 software (version 2.03.1). The PS-NP fluorescence was read at 360/460 nm (excitation/emission), and FD4 fluorescence was read at 485/528 nm (excitation/emission), with a gain of 50. FD4 and PS-NP standard curves prepared with stock FD4 solution and PS-NP dispersion respectively, and Krebs-Glucose were added on each plate and also read in duplicates. All standard curves had a $r^2 > 0.995$ for FD4, and $r^2 > 0.978$ for the PS-NP (see Supplementary material S3).

At each wavelength, the PS-NP concentration was calculated for each technical replicate as follows:

$$PS-NP\ Concentration_{\ Sample\ X} = \frac{(Fluo_{sample\ X} - Fluo_{Mean\ T0})}{a}$$

Where $Fluo_{Sample\ X}$ is the fluorescence read for the sample x (including sample at T0), $Fluo_{Mean\ T0}$ is the mean fluorescence read for all the samples at T0, and *a* is the slope of the straight-line y=*a*x of the standard curve.

The natural autofluorescence of the tissue was measured on median and distal segment during 150 min without any additional substance and was not considered as significant (Table S4).

Statistics on fluorescence data were performed on the mean $Concentration_{sample}$ values obtained from technical duplicates for each sample. Concentration data were analyzed with R (R Core

293 Team, 2020; version 3.6.1) using linear mixed-effects models (Package *nlme* version 3.1-140
294 (Pinheiro and Bates, 2000)) allowing for nested effects, using fish identification as a random
295 factor. The effect of gender was not tested because of the low number of males compared to
296 female samples. Pair-wise comparisons were performed using general linear hypothesis (glht)
297 in 'multcomp' package (Package *multcompView* version 0.1-8). A first model was used to test,
298 for each treatment (i.e. FD4, NP[20], NP[200]), if the two intestinal segments (median and
299 distal) differed significantly with regard to the substance concentration measured at each
300 sampling point compared to that measured at T0. This first model compared the kinetic
301 responses to a mean T0 calculated for both median and distal intestinal segments. To quantify
302 potential significant increase in concentration from T0 within each segment and treatment, a
303 second model was used for each segment independently, with a T0 calculated independently.
304 The models' conditions of application have been verified using qqnorm plots. Results are
305 presented as mean ± standard error.
306
307 2.4.2. *Sample preparation for further SEM and Py-GC-HRMS analyses*
308 To ensure that a potential fluorescence on the serosal side of the intestine sections is due to
309 translocation of NPs and not to leakage of the fluorophore, the solution from the serosal side of
310 the intestine (about 7 mL) was sampled at the end of the kinetic experiment (NP[200]
311 experiment, n=2 distal and n=2 median segments), and prepared to be analyzed by SEM and
312 Py-GC-HRMS. This serosal solution contained a lot of salts, present in the buffers used for the
313 experiment that can prevent further analyses because of their clumping potential (i.e.
314 agglutination potential), it was therefore necessary to remove them from the serosal solution.
315 For that, serosal samples were washed with trichloroacetic acid (TCA 10M) which separates
316 the beads from the salts by changing the polarity of the beads, and then facilitates their
317 precipitation by centrifugation commonly used for concentrating dilute protein/molecule

318 solutions and simultaneously removing undesirable substances (including salts and detergents,
319 Koontz, 2014). After a first centrifugation (20 min; 30,000 g), the pellet was dissolved in 1 mL
320 of filtered distilled water. TCA 99% was added (20% in volume, 10 M), and the solution was
321 centrifuged again (20 min; 30,000 g). The pellet was then resuspended in 1 mL of filtered
322 distilled water pending further analyses. The presence of fluorescence was controlled in the two
323 supernatant solutions and was about twice lower than in the pellet.
324
325 2.4.3. *Visual inspection by SEM*
326 After TCA precipitation, the solutions from the serosal sides of the distal and median segments
327 after injection of NP[200] [n = 2 for each segment]) were intended to be observed by SEM.
328 A volume of 6 mL was filtered through polycarbonate membranes (Millipore, 0.2 µm porosity).
329 Deposited samples were dried overnight in a laminar flow hood, fixed on aluminum stub with
330 a self-adhesive carbon pellet, and subsequently Au/Pd metallized under Ar flow using a sputter
331 coater Polaron SC7620. The SEM images were acquired on a SEM LEO 438VP.
332
333 2.4.4. *Py-GC-HRMS analyses*
334 In order to confirm the PS-NP composition of the beads observed, their chemical properties
335 were analyzed by Py-GC-HRMS. For that, a volume of 1 µL of pre-treated samples (from n=2
336 median; n=2 distal segments experiments, NP[200] experiment) was dropped off on quartz
337 discs into vials, previously cleaned at 1000°C and 2 quartz discs were added on top acting as a
338 cap. Samples were pyrolyzed at 600°C for 30 seconds with an autosampler of a CDS Pyroprobe
339 6150 (Oxford, US). For the transfer to gas chromatography GC, helium was used as carrier gas,
340 and temperatures of interface, valve oven and transfer line were set at 280°C, 300°C and 300°C,
341 respectively. The pyrolysis products were injected in a ThermoScientific Trace 1300 GC
342 (Villebon-sur-Yvette, France) with a temperature of 300°C and a split value of 5. Pyrolysis

products were separated using a RXi-5MS 15m x 0.25 mm x 0.25 µm column with a helium flow of 1.0 mL min^{-1}. The programmed oven temperature was as follows: 2 min at 40°C, then increased to 310°C at 9.0°C min^{-1}, hold for 10 min. Mass spectra were obtained with a ThermoScientific Q Exactive™ hybrid quadripole-Orbitrap mass spectrometer. All interfaces between GC and ionization source were maintained at 300°C and pyrolysis products were ionized at 70 eV and a mass range from 33.00000 to 500.00000 m/z with a resolution of 60,000. Specific markers of PS were particularly targeted using their ion markers: styrene (78.046 and 104.061 m/z), styrene dimer (91.054, 117.069, 193.101 and 208.125 m/z) and styrene trimer (91.054, 103.054, 195.112 and 312.187 m/z). A total of 10 blank samples were analyzed (3 pre-measure blanks, 4 intermediate blanks after each median or distal sample analyzed, and 3 post-measure blanks) to measure the basal signal of the laboratory, and thus check for the contaminations. The sample values were statistically compared to the blank values using a Wilcoxon rank sum test. The stock PS-NP dispersion was also analyzed. Results are presented as average area ± standard error.

3. Results

3.1. Time series of fluorescence

The higher the concentration of FD4 found in the serosal side, the greater its passage through the membrane, and the greater the impairment of membrane integrity (Thomson et al., 2019). The results obtained (Fig. 2) showed a FD4 concentration in the serosal part of both median and distal segments was was below the limit of detection (LOD; estimated at 23.4 ng mL^{-1}; see supplementary material to see the standard curves), so that it could not be detected. It did not increase over time neither in the distal nor in the median segment all along the experiment (p-values > 0.05, see sections 1.2.2, 1.3.2 of the S5 for FD4), proving the integrity of the intestinal tissue all along the 150 min experiment in both segments. Moreover this integrity was not

disturbed by addition of PS-NP (p-values > 0.05; see sections 2.2.2, 2.3.2 of S5 for FD4+NP20 and 3.2.2, 3.3.2 of S5 for FD4+NP200).

Results from fluorescence data show that PS-NP concentration in the serosal side of the intestinal sections increased from T0 within 15 minutes after addition of PS-NP to the luminal side in both the median and the distal sections (Fig. 3, and sections 4.3.2. and 5.2.2. of the S5). In median sections, PS-NP concentration after NP[200] addition reached a plateau after about 50 minutes (section 4.2.2 of S5), whereas that after NP[20] addition, PS-NP concentration continued to increase over 150 minutes and did not plateau (section 5.2.2 of S5). In distal sections, PS-NP concentration after NP[20] and NP[200] addition reached a plateau after only 15 minutes and there was no further increase up to 150 minutes (see sections 4.3.2. and 5.3.2. of S5). This difference between median and distal gut (p-value=0.0001; t-value=-4.457, see section 4.1.3) cannot be explained at this time but could result on the specialization of each of these intestinal segments in the assimilation process, considering that the median gut exhibits a higher pinocytosis ability that can accommodate smaller and hydrophobic particles such as polystyrene (Galloway et al., 2017; Urakami et al., 1994). For both median and distal segments, the final PS-NP concentrations measured in the serosal side were higher in NP[20] treatment than in NP[200] treatment compared to T0 (19-times and 17-times higher, respectively versus about 7-times and 4-times higher, respectively; p-value = 0.09, z-value = 2.831 for NP200 compared to T0, and p-value<0.001, z-value = 8.517 for NP20, see sections 4.1.1 and 5.1.1. respectively).

Fig. 2

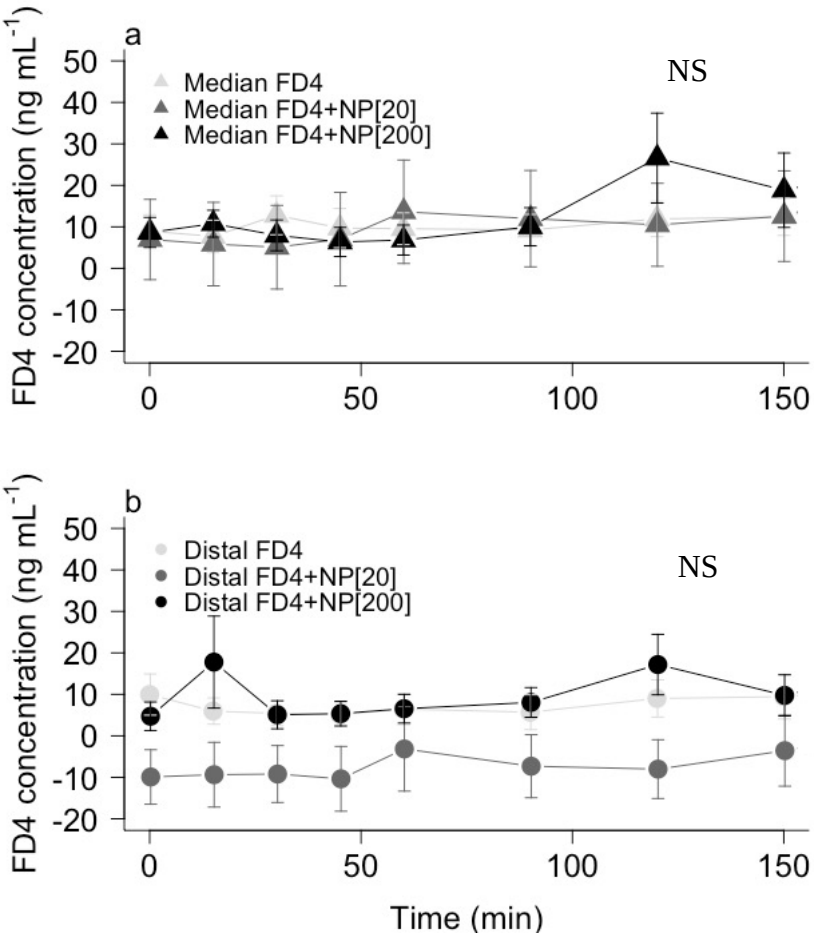

Fig. 2 : Kinetics of FD4 passage in the serous compartment of Ussing chambers as an indicator of gut integrity and permeability. FD4 concentration (ng $mL^{-1;}$ mean ± standard error) was measured over time in the serous side of the median (a) and distal (b) intestine of adult seabass (*Dicentrarchus labrax*) after addition of FD4 (initial concentration of 125 µg mL^{-1}; n=14 median intestines and n=15 distal intestines) into the luminal side of the tissue, and after combined addition of FD4 with two PS-NP concentration further tested (20 mg L^{-1}, i.e. NP[20], and 200 mg L^{-1}, i.e. NP[200]). The limit of detection (LOD) for FD4 was estimated at 23.4 ng mL^{-1} (see supplementary material S3 to see the standard curves). NS indicates no significant differences from T0, nor from each other sampling point whatever the treatments (linear mixed-effect model and general linear hypothesis with *glht*() in 'mutlcomp' package, see sections 1 and 2,in supplementary material S5).

404 **Fig. 3**

405

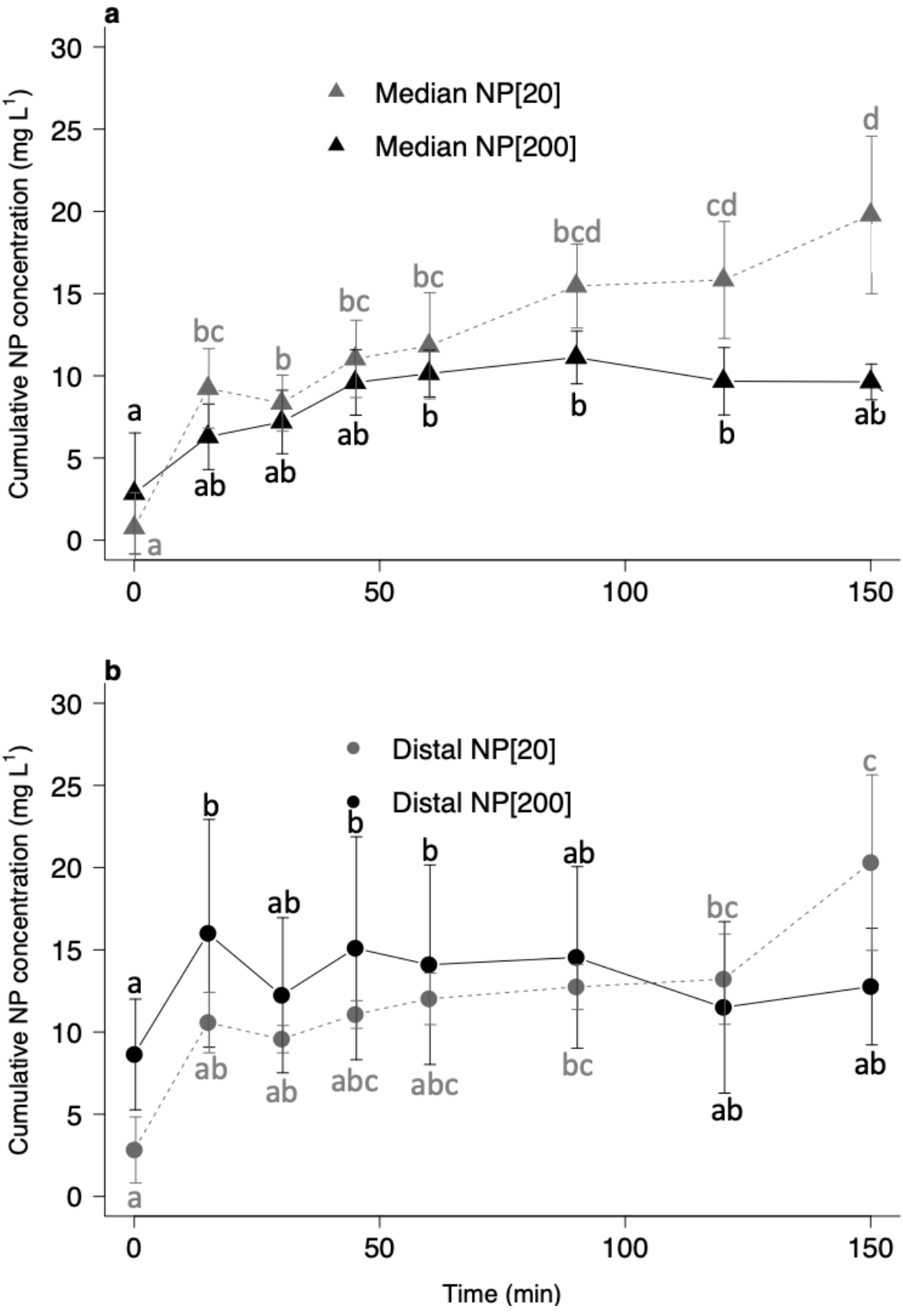

406

Fig. 3 : Kinetics of 50 nm polystyrene nanoplastic beads (NP) passage in the serosal part of median and distal gut segments. NP concentration (mg L^{-1}; mean ± standard error) measured in the serous side of the median (a) and distal (b) intestine of adult seabass (*Dicentrarchus labrax*) after addition of pure NP at two concentrations (either 20 mg L^{-1} or 200 mg L^{-1}, n=6 per intestinal segment) in the luminal side. For each NP concentration, means not sharing a common letter are significantly different (linear mixed-effect model and general linear hypothesis with *glht* in 'mutlcomp' package, see supplementary material section 4 and 5 of the S5 for detailed statistical results). Fluorescence is not null at T0 because of the natural fluorescence of the composed solutions used. This value T0 has been subtracted from the others (see material and methods section). The limit of detection (LOD) for PS-NP was estimated at 9.2 mg L^{-1} (See supplementary material to see the standard curves).

3.2. SEM analyses on serosal samples

However, it is important to note that the increasing PS-NP concentrations calculated from increasing fluorescence cannot be undoubtedly interpreted by a passage of PS-NP, as a leakage of fluorophore from the beads may have occurred, all along the experiment (including in the Krebs-Mannitol solution). The control of leakage by dialysis protocol revealed about 20% of dye leakage (see supplementary material S2), supporting the need to use other techniques and not only fluorescence to reveal the presence of PS-NP in the serous side.

The SEM analyses revealed an agglutination of beads that was due to the TCA precipitation protocol used, as the same was observed concerning the stock solution of fluorescent PS–NP beads treated with TCA (Fig. 4). Also, a DLS analysis helped to confirm that after TCA washing

protocol, beads formed microscale aggregates (2351.3 ± 511.7 nm), displaying a negative surface charge (-5.1 ± 0.6 mV), while they remained at a nanometric scale with a positive surface charge in ultrapure water (66.1 ± 0.4 nm and 51.4 ± 2.1 mV), 10 mM Krebs-Glucose (306.2 ± 61.1 nm and 19.4 ± 1.1 mV) and 10 mM Krebs-Mannitol (86.0 ± 0.4 nm and 18.5 ± 3.5 mV), used during the experiment. These results showed that most of the translocated fluorescence observed was due to beads and not to leached fluorescence. Observing beads in the median sample was technically challenging considering that the quality of the wash and TCA precipitation was not optimal.

Fig. 4

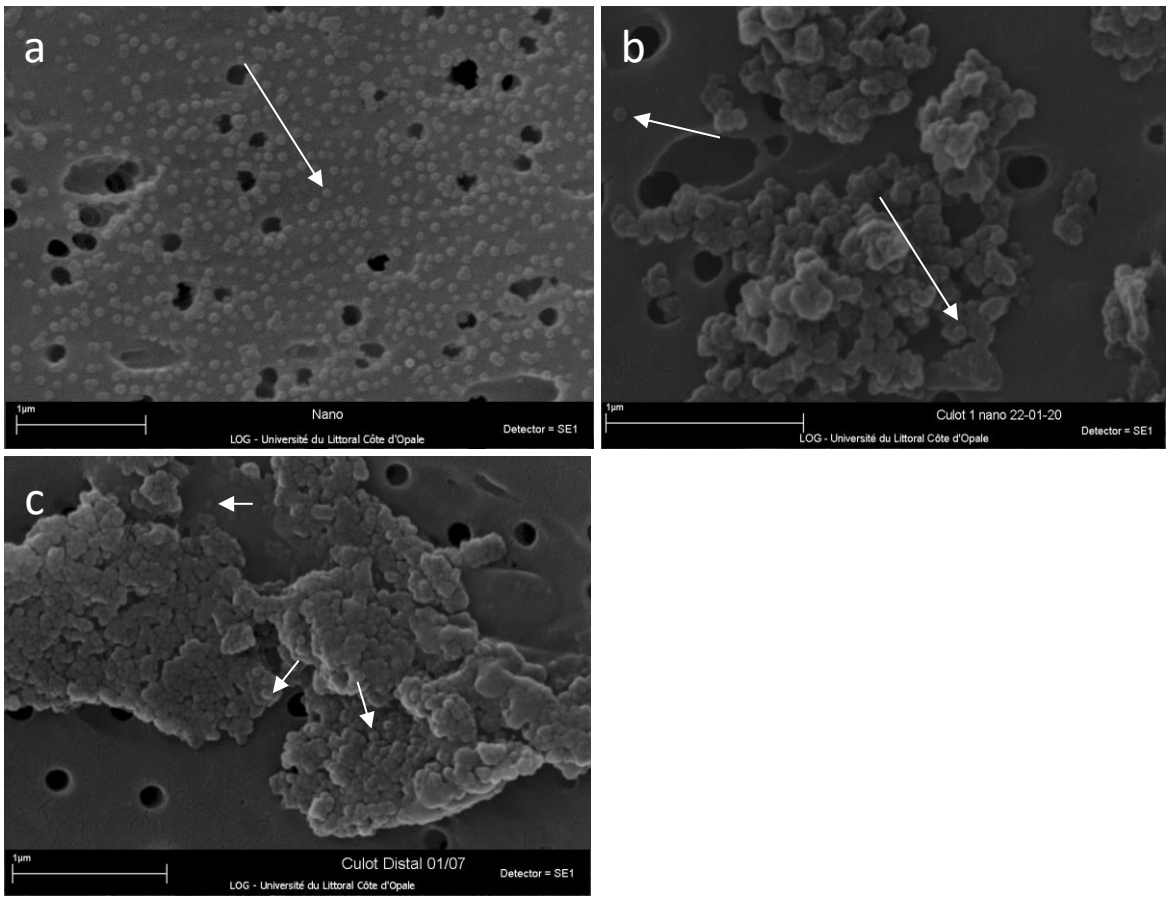

Fig. 4 : Observation of nanoplastics by scanning electron microscopy. (a) Sample of aqueous suspension of polystyrene nanoplastic beads (PS-NP) at the concentration of 5000 mg L^{-1} in Krebs-Glucose (latex beads amine-modified polystyrene 0.05 µm mean particle size, Sigma-Aldrich, France); (b) sample of the same aqueous PS-NP dispersion after the TCA precipitation protocol (see details in material and methods section); (c) sample of Krebs-Glucose solution collected from the serous side of the distal portion of the intestine, at the end of the 150-min kinetic experiment during which the PS-NP dispersion diluted at 200 mg L^{-1} was added to the luminal side at T0, and washed according to the TCA precipitation protocol. The white arrows show the nanoplastic beads observed.

3.3. Particles characterisation via Py-GC-HRMS analyses

At the end of this set of analysis, it remained to ascertain the polymeric composition of the beads by analyzing the pyrolysis products generated by Py-GC-HRMS (Table 1). The pyrolysis product of the PS-NP stock dispersion showed a strong signal of styrene and a weaker signal of styrene dimer (at such high pyrolysis temperature styrene trimer was nearly absent). Consequently, the styrene was conserved as the unique target marker for PS-NP. Substantial amounts of styrene were identified in the samples taken from the serosal side of both the median (surface area: 379,574,179 ± 198,468,159) and distal (surface area : 398,258,238 ± 363,810,422) intestine sections after addition of NP[200]. No significant difference in these chemical properties was observed between median and distal intestinal segments.

Table 1: Styren signal intensities measured by Py-GC-HRMS in the serosal solutions (Krebs-Glucose) collected from the serous side of the distal (n=2) and median (n=2) portions of the intestine compared to the PS-NP stock dispersion (n=1). Data are expressed as a mean ± standard error.

	Styrene surface area (arbitrary unit, mean area ± standard error)
PS-NP stock dispersion	16 804 278 980
Blank (n=10)	4 501 980 ± 869 945
Median gut (n = 2)	**379 574 179 ± 198 468 159**
Distal gut (n = 2)	**398 258 238 ± 363 810 422**

Before analyses, serosal solutions were washed according to the TCA precipitation protocol, at the end of the kinetic experiment in Ussing chambers during which the 50 nm polystyrene nanoplastic (PS-NP) beads dispersion diluted at 200 mg L^{-1} was tested. The PS-NP stock

dispersion was not treated with the TCA protocol before analyses. The 10 blank values in total contain n=3 pre-measure blanks, n=4 intermediate blanks and n = 3 post-measure blanks. The absence of standard error indicates that no second value was obtained. The bold values are significantly different from the blank value (Wilcoxon test, W = 40, p-value < 0.001). Only the styrene was statistically analyzed because it was the most important peak of the tested solutions, the remaining peaks were represented by styrene dimer and trimer.

4. Discussion

4.1. *Strengths of combining techniques for monitoring nanometric particles in tissues.*

By coupling fluorescence, SEM and Py-GC/HRMS, completed by DLS analyses, the present study evidences the translocation of 50 nm, -NH_2 functionalized PS-NP nanobeads, across the intestine of adult European sea bass. This was presumably due to the fact that they remained in the nanometre state in both Krebs-Mannitol and Krebs-Glucose as shown by the DLS analyses. Indeed, they were only aggregated with TCA precipitation.

First, by measuring the increase in fluorescence on the serosal side of the intestine, we found a regular increase of PS-NP concentration, even if less marked from 90 min, in the serosal side of both median and distal segments of the intestine, after injection of 200 mg L^{-1} and 20 mg L^{-1} PS-NP (NP[20] and NP[200]) in the luminal side, suggesting a passage of PS-NP. Second, SEM provided additional visual proof of the passage of PS-NP through the distal intestinal segment at the PS-NP concentration of 200 mg L^{-1} (NP[200]). And third, Py-GC/HRMS data clearly showed that the amount of styrene in the samples was 4–90-times greater when compared to the controls after intestinal luminal exposure to this concentration, confirming the presence of PS in both median and distal samples, rather than leaching of fluorescence.

The aggregates of PS-NP observed by electron microscopy on the experimental samples can be seen as an artefact of our methodologies because the TCA used to remove the salts to ensure

SEM good quality caused a shift in the ζ-potential leading to aggregation, while the PS-NP remained at a nanometre state during exposures as confirmed by DLS. Although an improvement of the methodology is certainly possible to avoid this aggregation, this does not compromise the demonstration of the passage of PS-NPs through the intestinal epithelium. This shows that using complementary methods is necessary to prove and to carefully interpret the presence of PS-NP on the serosal part of the intestine.

Surprisingly, for both median and distal segments, the final PS-NP concentrations measured in the serosal side were higher in NP[20] treatment than in NP[200] treatment compared to T0. This could be due to an overloading at the highest NP concentrations, possibly resulting in a shutdown of the absorptive capacity as reported several years ago in grasscarp, *Ctenopharyngodon idella*, when large amounts of food are suddenly available (Stroband and van der Veen, 1981). It is not excluded that a concentration-dependent aggregation may have also played a role inducing a bias for a non-constant exposure, but DLS data indicated that NP remained in the nanometric scale after 15-30 min of incubation in the four media used in this study. Additionally, we know that these NPs have a stable behavior over 48h in ultrapure water, artificial seawater and 2-mm filtered natural (Tallec et al., 2019).

Our study makes it possible to resolve issues raised in a very recent study reporting the translocation of PS-NP palladium labelled through the intestine of another fish species, the Atlantic salmon *Salmo salar* (Clark et al., 2022). Clark's study and our study proposed different ways to address the debated issue of PS-NP translocation. First, we used three complementary methods to evidence the PS-NP translocation in a direct manner, whereas Clark et al. showed the presence of PS-NP-palladium labelled measuring palladium by inductively coupled plasma mass spectrometry (ICP-MS). Second, we confirmed the PS-NP passage through median and distal intestinal segments, whereas Clark et al. found a passage in the anterior intestine, containing pyloric caeca. This accumulation of PS-NP in anterior intestine would be a

consequence of the nature of pyloric caeca, which is a region of bacteria translocation through endocytosis (Ringø et al., 2007), which is the same mechanism as nanoparticle uptake. Pyloric caeca, by their structure, could thus represent a slightly different and very specific portion of the intestine that could favor translocation. Therefore, it may not be representative of the entire intestine of all vertebrates, which are generally devoid of such structures. Third, our study shows the passage of PS-NP through an intact and functional intestine, as proven by the FD4 experiment (Fig. 1). Our results showed the integrity of the membrane all along the experiment, and that this integrity was not disturbed by addition of PS-NP. In Clark et al. the ligations performed on both sides of the intestine could have favored local necrosis and consequently the passage of PS-NP, though this should be confirmed. Finally, the Ussing chamber we used has long been recognized as the most *ex-vivo* suitable method to study the transport processes, while Clark et al. recognize “the limitations of the gut sac method” and call for complementary innovative methods to their "proof-of-concept study".

4.2. *Limitations of our study*

However, we are aware that our experimental design imposes some limitations on data interpretation.

First, we used manufactured standardized polystyrene latex beads with a round regular shape, whereas in natural marine habitats, nanoplastic debris vary in shape and composition (e.g. polyethylene, polyester), and surface state (microorganisms and biomolecules attached to the plastic surface, i.e. eco-corona), and these three factors may play a role in translocation (Ramsperger et al., 2020; Rochman et al., 2019). For example, the styrene content of polystyrene microplastics has been shown to strongly influence their ability to be phagocytized: the greater the styrene content, the greater their ability to undergo phagocytosis (Urakami et al., 1994). Also, the surface functionalization of the PS-NP (NH_2 in the present study) can affect

the physical behavior of the particles (e.g. aggregation, charge) in solution (Tallec et al., 2019), and can consequently modify their bioavailability and thus their toxicity (Tallec et al., 2018). The functionalization and surface charge are responsible for the interfacial dynamics, and thus the interactions with living systems, especially biological membranes (Corsi et al., 2020). Electrostatic interactions produced by the positive charges, such as NH_2, can reorient the phospholipid headgroups of membranes, reducing lipid density and fluidizing the membrane (Liu et al., 2020, 2011). This facilitates both passive diffusion and the membrane bending associated with endo- and phagocytosis (Matthews et al., 2021), and can contribute to the fast uptake of the PS-NH_2. Moreover, the environmental relevance of NH_2-functionalized NP is questionable due to oxidation processes occurring in the environment leading to a carboxylic surface and anionic charge (Fotopoulou and Karapanagioti, 2012).

Second, we showed a translocation process from 15 min after addition into the luminal side, but this time does not consider the natural transit time of the particles along the gut. In mussels, the translocation of plastic particles (particles of 3 and 9.6 µm) *in vivo* was estimated to start 3 days after ingestion, and was highest 12 days after ingestion. Smaller particles (3 µm) were much more translocated than larger ones (9.6 µm) suggesting an interaction "translocation time x particle size" that remains to be tested. Then, further experiments are required to validate our findings *in vivo* in fish living in natural environment.

Finally, in order to avoid excessive manipulation of the intestinal segment that could have impaired tissue integrity, the muscle layers were not dissected out. Therefore, the NP and FD4 passages measured in our set-up are probably underestimated since these molecules have more cell layers to cross before reaching the serosal compartment, compared to the *in vivo* situation where the molecules would reach the bloodstream more rapidly.

We are aware that the fluorescence measurement method has biases and we wanted to add methods like SEM and Py-GC/HMRS, but which are not quantitative. Anyway, our idea was

to make the proof of concept that there is a passage but not to quantify this passage because the Ussing method is too 'artificial' (e.g. no intestinal transit, nor blood flow, nor hormonal or nervous influence in Ussing chambers).

5. Conclusion

This study reports direct evidence from an *ex vivo* system that translocation of 50 nm PS-NPs across the intestine of the European sea bass occurs within a few minutes. Previous studies showed the presence of NPs in various tissues, but either no clear or indirect evidence of translocation was provided, or the data were compromised by inadequate tissue preparation or methodology. Also, our study makes it possible to resolve issues raised in a very recent study reporting the translocation in another fish species. The findings of our present study are strengthened by the combination of fluorescence measurements, insufficient alone because of possible fluorophore leaching, with two complementary analytical methods that proved the physical presence of PS-NP on the serosal side of the intestine. Our data reveal that NPs beads can be translocated across the intestinal barrier in the medial and distal intestine. This provides a plausible mechanism to explain the appearance of NPs in internal organs by subsequent transportation through the bloodstream.

References

Abbasi, S., Soltani, N., Keshavarzi, B., Moore, F., Turner, A., Hassanaghaei, M., 2018. Microplastics in different tissues of fish and prawn from the Musa Estuary, Persian Gulf. Chemosphere 205, 80–87. https://doi.org/10.1016/j.chemosphere.2018.04.076

Ašmonaitė, G., Sundh, H., Asker, N., Carney Almroth, B., 2018. Rainbow Trout Maintain Intestinal Transport and Barrier Functions Following Exposure to Polystyrene Microplastics. Environ. Sci. Technol. 52, 14392–14401. https://doi.org/10.1021/acs.est.8b04848

Barrington, E.J.W., 1957. THE ALIMENTARY CANAL AND DIGESTION, in: The Physiology of Fishes. Elsevier, pp. 109–161. https://doi.org/10.1016/B978-1-4832-2817-4.50009-3

Brandon, J.A., Freibott, A., Sala, L.M., 2020. Patterns of suspended and salp-ingested microplastic debris in the North Pacific investigated with epifluorescence microscopy. Limnol Oceanogr Letters 5, 46–53. https://doi.org/10.1002/lol2.10127

Catarino, A.I., Frutos, A., Henry, T.B., 2019. Use of fluorescent-labelled nanoplastics (NPs) to demonstrate NP absorption is inconclusive without adequate controls. Science of The Total Environment 670, 915–920. https://doi.org/10.1016/j.scitotenv.2019.03.194
Clark, N.J., Khan, F.R., Mitrano, D.M., Boyle, D., Thompson, R.C., 2022. Demonstrating the translocation of nanoplastics across the fish intestine using palladium-doped polystyrene in a salmon gut-sac. Environment International 159, 106994. https://doi.org/10.1016/j.envint.2021.106994
Clarke, L.L., 2009. A guide to Ussing chamber studies of mouse intestine. American Journal of Physiology-Gastrointestinal and Liver Physiology 296, G1151–G1166. https://doi.org/10.1152/ajpgi.90649.2008
Collard, F., Gilbert, B., Compère, P., Eppe, G., Das, K., Jauniaux, T., Parmentier, E., 2017. Microplastics in livers of European anchovies (Engraulis encrasicolus , L.). Environmental Pollution 229, 1000–1005. https://doi.org/10.1016/j.envpol.2017.07.089
Corsi, I., Bergami, E., Grassi, G., 2020. Behavior and Bio-Interactions of Anthropogenic Particles in Marine Environment for a More Realistic Ecological Risk Assessment. Front. Environ. Sci. 8, 60. https://doi.org/10.3389/fenvs.2020.00060
de Jonge, H.R., Ballmann, M., Veeze, H., Bronsveld, I., Stanke, F., Tümmler, B., Sinaasappel, M., 2004. Ex vivo CF diagnosis by intestinal current measurements (ICM) in small aperture, circulating Ussing chambers. Journal of Cystic Fibrosis 3, 159–163. https://doi.org/10.1016/j.jcf.2004.05.034
Ding, J., Zhang, S., Razanajatovo, R.M., Zou, H., Zhu, W., 2018. Accumulation, tissue distribution, and biochemical effects of polystyrene microplastics in the freshwater fish red tilapia (Oreochromis niloticus). Environmental Pollution 238, 1–9. https://doi.org/10.1016/j.envpol.2018.03.001
Elizalde-Velázquez, A., Crago, J., Zhao, X., Green, M.J., Cañas-Carrell, J.E., 2020. In vivo effects on the immune function of fathead minnow (Pimephales promelas) following ingestion and intraperitoneal injection of polystyrene nanoplastics. Science of The Total Environment 735, 139461. https://doi.org/10.1016/j.scitotenv.2020.139461
Fotopoulou, K.N., Karapanagioti, H.K., 2012. Surface properties of beached plastic pellets. Marine Environmental Research 81, 70–77. https://doi.org/10.1016/j.marenvres.2012.08.010
Galloway, T.S., Cole, M., Lewis, C., 2017. Interactions of microplastic debris throughout the marine ecosystem. Nat Ecol Evol 1, 0116. https://doi.org/10.1038/s41559-017-0116
Gonçalves, J.M., Bebianno, M.J., 2021. Nanoplastics impact on marine biota: A review. Environmental Pollution 273, 116426. https://doi.org/10.1016/j.envpol.2021.116426
Grosell, M., Genz, J., 2006. Ouabain-sensitive bicarbonate secretion and acid absorption by the marine teleost fish intestine play a role in osmoregulation. American Journal of Physiology-Regulatory, Integrative and Comparative Physiology 291, R1145–R1156. https://doi.org/10.1152/ajpregu.00818.2005
Guffey, S., Esbaugh, A., Grosell, M., 2011. Regulation of apical H^+-ATPase activity and intestinal HCO_3^- secretion in marine fish osmoregulation. American Journal of Physiology-Regulatory, Integrative and Comparative Physiology 301, R1682–R1691. https://doi.org/10.1152/ajpregu.00059.2011
Gutow, L., Eckerlebe, A., Giménez, L., Saborowski, R., 2016. Experimental Evaluation of Seaweeds as a Vector for Microplastics into Marine Food Webs. Environ. Sci. Technol. 50, 915–923. https://doi.org/10.1021/acs.est.5b02431
Haslam, I.S., O'Reilly, D.A., Sherlock, D.J., Kauser, A., Womack, C., Coleman, T., 2011. Pancreatoduodenectomy as a source of human small intestine for Ussing chamber investigations and comparative studies with rat tissue. Biopharm. Drug Dispos. 32, 210–221. https://doi.org/10.1002/bdd.751
Jovanović, B., Gökdağ, K., Güven, O., Emre, Y., Whitley, E.M., Kideys, A.E., 2018. Virgin

667 microplastics are not causing imminent harm to fish after dietary exposure. Marine Pollution
668 Bulletin 130, 123–131. https://doi.org/10.1016/j.marpolbul.2018.03.016
669 Kapoor, B.G., Smit, H., Verighina, I.A., 1976. The Alimentary Canal and Digestion in
670 Teleosts, in: Advances in Marine Biology. Elsevier, pp. 109–239.
671 https://doi.org/10.1016/S0065-2881(08)60281-3
672 Kim, J., Poirier, D.G., Helm, P.A., Bayoumi, M., Rochman, C.M., 2020. No evidence of
673 spherical microplastics (10–300 μm) translocation in adult rainbow trout (Oncorhynchus
674 mykiss) after a two-week dietary exposure. PLoS ONE 15, e0239128.
675 https://doi.org/10.1371/journal.pone.0239128
676 Koontz, L., 2014. TCA Precipitation, in: Methods in Enzymology. Elsevier, pp. 3–10.
677 https://doi.org/10.1016/B978-0-12-420119-4.00001-X
678 Liu, Y., Huang, Z., Zhou, J., Tang, J., Yang, C., Chen, C., Huang, W., Dang, Z., 2020.
679 Influence of environmental and biological macromolecules on aggregation kinetics of
680 nanoplastics in aquatic systems. Water Research 186, 116316.
681 https://doi.org/10.1016/j.watres.2020.116316
682 Liu, Yuexian, Li, W., Lao, F., Liu, Ying, Wang, L., Bai, R., Zhao, Y., Chen, C., 2011.
683 Intracellular dynamics of cationic and anionic polystyrene nanoparticles without direct
684 interaction with mitotic spindle and chromosomes. Biomaterials 32, 8291–8303.
685 https://doi.org/10.1016/j.biomaterials.2011.07.037
686 Matthews, S., Mai, L., Jeong, C.-B., Lee, J.-S., Zeng, E.Y., Xu, E.G., 2021. Key mechanisms
687 of micro- and nanoplastic (MNP) toxicity across taxonomic groups. Comparative
688 Biochemistry and Physiology Part C: Toxicology & Pharmacology 247, 109056.
689 https://doi.org/10.1016/j.cbpc.2021.109056
690 Mattsson, K., Johnson, E.V., Malmendal, A., Linse, S., Hansson, L.-A., Cedervall, T., 2017.
691 Brain damage and behavioural disorders in fish induced by plastic nanoparticles delivered
692 through the food chain. Sci Rep 7, 11452. https://doi.org/10.1038/s41598-017-10813-0
693 Ostroumov, S.A., 2003. Studying effects of some surfactants and detergents on filter-feeding
694 bivalves. Hydrobiologia 500, 341–344. https://doi.org/10.1023/A:1024604904065
695 Paul-Pont, I., Tallec, K., Gonzalez-Fernandez, C., Lambert, C., Vincent, D., Mazurais, D.,
696 Zambonino-Infante, J.-L., Brotons, G., Lagarde, F., Fabioux, C., Soudant, P., Huvet, A., 2018.
697 Constraints and Priorities for Conducting Experimental Exposures of Marine Organisms to
698 Microplastics. Front. Mar. Sci. 5, 252. https://doi.org/10.3389/fmars.2018.00252
699 Pinheiro, J.C., Bates, D.M., 2000. Mixed-Effects Models in Sand S-PLUS, Statistics and
700 Computing. Springer New York, New York, NY. https://doi.org/10.1007/978-1-4419-0318-1
701 Pitt, J.A., Kozal, J.S., Jayasundara, N., Massarsky, A., Trevisan, R., Geitner, N., Wiesner, M.,
702 Levin, E.D., Di Giulio, R.T., 2018a. Uptake, tissue distribution, and toxicity of polystyrene
703 nanoparticles in developing zebrafish (Danio rerio). Aquatic Toxicology 194, 185–194.
704 https://doi.org/10.1016/j.aquatox.2017.11.017
705 Pitt, J.A., Trevisan, R., Massarsky, A., Kozal, J.S., Levin, E.D., Di Giulio, R.T., 2018b.
706 Maternal transfer of nanoplastics to offspring in zebrafish (Danio rerio): A case study with
707 nanopolystyrene. Science of The Total Environment 643, 324–334.
708 https://doi.org/10.1016/j.scitotenv.2018.06.186
709 Ramsperger, A.F.R.M., Narayana, V.K.B., Gross, W., Mohanraj, J., Thelakkat, M., Greiner,
710 A., Schmalz, H., Kress, H., Laforsch, C., 2020. Environmental exposure enhances the
711 internalization of microplastic particles into cells. Sci. Adv. 6.
712 https://doi.org/10.1126/sciadv.abd1211
713 Ringø, E., Myklebust, R., Mayhew, T.M., Olsen, R.E., 2007. Bacterial translocation and
714 pathogenesis in the digestive tract of larvae and fry. Aquaculture 268, 251–264.
715 https://doi.org/10.1016/j.aquaculture.2007.04.047
716 Rochman, C.M., Brookson, C., Bikker, J., Djuric, N., Earn, A., Bucci, K., Athey, S.,

Huntington, A., McIlwraith, H., Munno, K., De Frond, H., Kolomijeca, A., Erdle, L., Grbic, J., Bayoumi, M., Borrelle, S.B., Wu, T., Santoro, S., Werbowski, L.M., Zhu, X., Giles, R.K., Hamilton, B.M., Thaysen, C., Kaura, A., Klasios, N., Ead, L., Kim, J., Sherlock, C., Ho, A., Hung, C., 2019. Rethinking microplastics as a diverse contaminant suite. Environ Toxicol Chem 38, 703–711. https://doi.org/10.1002/etc.4371

Schür, C., Rist, S., Baun, A., Mayer, P., Hartmann, N.B., Wagner, M., 2019. When Fluorescence Is not a Particle: The Tissue Translocation of Microplastics in *Daphnia magna* Seems an Artifact. Environ Toxicol Chem 38, 1495–1503. https://doi.org/10.1002/etc.4436

Stroband, H.W.J., van der Veen, F.H., 1981. Localization of protein absorption during transport of food in the intestine of the grasscarp,Ctenopharyngodon idella (Val.). J. Exp. Zool. 218, 149–156. https://doi.org/10.1002/jez.1402180207

Tallec, K., Blard, O., González-Fernández, C., Brotons, G., Berchel, M., Soudant, P., Huvet, A., Paul-Pont, I., 2019. Surface functionalization determines behavior of nanoplastic solutions in model aquatic environments. Chemosphere 225, 639–646. https://doi.org/10.1016/j.chemosphere.2019.03.077

Tallec, K., Huvet, A., Di Poi, C., González-Fernández, C., Lambert, C., Petton, B., Le Goïc, N., Berchel, M., Soudant, P., Paul-Pont, I., 2018. Nanoplastics impaired oyster free living stages, gametes and embryos. Environmental Pollution 242, 1226–1235. https://doi.org/10.1016/j.envpol.2018.08.020

Tallec, K., Paul-Pont, I., Petton, B., Alunno-Bruscia, M., Bourdon, C., Bernardini, I., Boulais, M., Lambert, C., Quéré, C., Bideau, A., Le Goïc, N., Cassone, A.-L., Le Grand, F., Fabioux, C., Soudant, P., Huvet, A., 2021. Amino-nanopolystyrene exposures of oyster (*Crassostrea gigas*) embryos induced no apparent intergenerational effects. Nanotoxicology 1–17. https://doi.org/10.1080/17435390.2021.1879963

Thomson, A., Smart, K., Somerville, M.S., Lauder, S.N., Appanna, G., Horwood, J., Sunder Raj, L., Srivastava, B., Durai, D., Scurr, M.J., Keita, Å.V., Gallimore, A.M., Godkin, A., 2019. The Ussing chamber system for measuring intestinal permeability in health and disease. BMC Gastroenterol 19, 98. https://doi.org/10.1186/s12876-019-1002-4

Triebskorn, R., Braunbeck, T., Grummt, T., Hanslik, L., Huppertsberg, S., Jekel, M., Knepper, T.P., Krais, S., Müller, Y.K., Pittroff, M., Ruhl, A.S., Schmieg, H., Schür, C., Strobel, C., Wagner, M., Zumbülte, N., Köhler, H.-R., 2019. Relevance of nano- and microplastics for freshwater ecosystems: A critical review. TrAC Trends in Analytical Chemistry 110, 375–392. https://doi.org/10.1016/j.trac.2018.11.023

Urakami, Y., Kasuya, Y., Fujimoto, K., Miyamoto, M., Kawaguchi, H., 1994. Phagocytosis of microspheres with modified surfaces. Colloids and Surfaces B: Biointerfaces 3, 183–190. https://doi.org/10.1016/0927-7765(94)80065-0

Ussing, H.H., Zerahn, K., 1951. Active Transport of Sodium as the Source of Electric Current in the Short-circuited Isolated Frog Skin. Acta Physiologica Scandinavica 23, 110–127. https://doi.org/10.1111/j.1748-1716.1951.tb00800.x

van Pomeren, M., Brun, N.R., Peijnenburg, W.J.G.M., Vijver, M.G., 2017. Exploring uptake and biodistribution of polystyrene (nano)particles in zebrafish embryos at different developmental stages. Aquatic Toxicology 190, 40–45. https://doi.org/10.1016/j.aquatox.2017.06.017

Volkheimer, G., 1975. Hematogenous dissemination of ingested polyvinyl chloride particles. Ann N Y Acad Sci 246, 164–171. https://doi.org/10.1111/j.1749-6632.1975.tb51092.x

Volkheimer, G., 1974. Passage of particles through the wall of the gastrointestinal tract. Environmental Health Perspectives 9, 215–225. https://doi.org/10.2307/3428287

Wagner, S., Reemtsma, T., 2019. Things we know and don’t know about nanoplastic in the environment. Nat. Nanotechnol. 14, 300–301. https://doi.org/10.1038/s41565-019-0424-z

Weinrauch, A.M., Hoogenboom, J.L., Anderson, W.G., 2021. A review of reductionist

methods in fish gastrointestinal tract physiology. Comparative Biochemistry and Physiology Part B: Biochemistry and Molecular Biology 254, 110571. https://doi.org/10.1016/j.cbpb.2021.110571
Zeytin, S., Wagner, G., Mackay-Roberts, N., Gerdts, G., Schuirmann, E., Klockmann, S., Slater, M., 2020. Quantifying microplastic translocation from feed to the fillet in European sea bass Dicentrarchus labrax. Marine Pollution Bulletin 156, 111210. https://doi.org/10.1016/j.marpolbul.2020.111210

Acknowledgements

Authors thank L. Madec and M.M. Le Gall for their technical help with Ussing chambers, S. Collet for her help with rearing animals, C. Thorin for her help with statistical analyses, V. Loizeau for her help with the interpretation of chemical results, and C. Himber for sample preparation for Py-GC-HRMS. We acknowledge I. Paul-Pont and P. Soudant for discussions during the course of this work and PA. Jaffres and O. Lozach (UMR-CNRS 6521) for the use of their equipment for DLS analyses. We acknowledge Life Science Editors for professional scientific editing services during the preparation of the manuscript.

Funding

This work was supported by the French National Research Agency, project Nanoplastics 15-CE34-0006 (2016-2021). Part of this work was also funded by the European Union (European Regional Development Fund), the French government, the Hauts-de-France Regional Council (in the framework of the CPER MARCO project 2015-2020) and Ifremer (Institut Français de Recherche pour l'Exploitation de la Mer).

CRediT authorship contribution statement

All of the authors contributed to writing and editing the manuscript. M. Vagner. performed the experiment, analyzed the data; G. Boudry designed the analysis; L. Courcot performed the scanning electron microscopy ; D.Vincent and A. Huvet advised on the methodology regarding NP concentrations and detection strategies; K. Tallec performed the DLS analyses; G. Duflos

796 performed the management of Py-GC-HRMS; A. Dehaut. performed the Py-GC-HRMS data
797 treatments; J.-L. Zambonino. designed and performed the experiment and analyzed the data.
798
799 **Declaration of Competing Interest**
800 The authors declare no conflicts of interest.
801
802 **List of supplementary materials**
803 **Supplementary material S1 Testing the adsorption of FD4 to PS-NP**
804 **Supplementary material S2: Control for leakage of dye by dialysis**
805 **Supplementary material S3 : Calibration curves**
806 **Supplementary material S4: Determination of the autofluorescence of the tissue**
807 **Supplementary material S5 : Statistical analyses of the fluorescence dataset**
808
809
810
811
812
813